

Advance Access Publication Date: Day Month Year

Original article

Quantifying Periodicity in Non-Euclidean Random Objects

Jiazen Xu,^{1,*} Andrew T. A. Wood² and Tao Zou²

¹Department of Actuarial Studies and Business Analytics , Macquarie University, 2113, NSW, Australia

and ²Research School of Finance, Actuarial Studies and Statistics, Australian National University, 2600, ACT, Australia

*Address for correspondence. Jiazen Xu, Department of Actuarial Studies and Business Analytics, Macquarie University, Sydney, 2113, Australia. jiazen.xu@mq.edu.au

FOR PUBLISHER ONLY Received on Date Month Year; revised on Date Month Year; accepted on Date Month Year

Abstract

Time-varying non-Euclidean random objects are playing a growing role in modern data analysis, and periodicity is a fundamental characteristic of time-varying data. However, quantifying periodicity in general non-Euclidean random objects remains largely unexplored. In this work, we introduce a novel nonparametric framework for quantifying periodicity in random objects within a general metric space that lacks Euclidean structures. Our approach formulates periodicity estimation as a model selection problem and provides methodologies for period estimation, data-driven tuning parameter selection, and periodic component extraction. Our theoretical contributions include establishing the consistency of period estimation without relying on linearity properties used in the literature for Euclidean data, providing theoretical support for data-driven tuning parameter selection, and deriving uniform convergence results for periodic component estimation. Through extensive simulation studies covering three distinct types of time-varying random objects such as compositional data, networks, and functional data, we showcase the superior accuracy achieved by our approach in periodicity quantification. Finally, we apply our method to various real datasets, including U.S. electricity generation compositions, New York City transportation networks, and Germany's water consumption curves, highlighting its practical relevance in identifying and quantifying meaningful periodic patterns.

Key words: Fréchet Regression, Information Criteria, Metric Space, Model Selection, Non-Euclidean Data, Tuning Parameter Selection

1. Introduction

Advances in data collection technologies have made the acquisition of random object data increasingly common (Marron and Dryden 2021). Examples include networks, phylogenetic trees, probability distribution functions, covariance matrices, compositional data, and spherical data (Worsley et al. 2002; Kolar et al. 2010; Scealy and Wood 2023). These data types frequently arise in various applications and are often observed over time, resulting in time-varying random objects indexed by temporal grids (Dubey and Müller 2021). Time-varying random objects often reside in general metric spaces rather than Euclidean spaces, which limits the applicability of traditional statistical methods. Unlike Euclidean spaces, general metric spaces often lack linear structures and vector space operations are not defined, posing significant challenges for traditional data analytical methods.

Periodic patterns are frequently observed in time-varying random objects. For instance, Hörmann et al. (2018) study periodicity in time-varying functions, identifying weekly cycles in daily air pollution curves caused by weekday-dependent traffic patterns in Graz, Austria. Xu et al. (2025) observe periodic behaviour of time-varying transportation networks in New York City. Dynamic transportation networks observed on an hourly basis are influenced by rush hour patterns, resulting in periodicity with period being assumed to be twenty-four hours.

Additional examples of periodic random objects appear in contexts such as monthly electricity generation and social communication networks. For electricity generation data, each monthly observation represents the percentage contribution of a source to net generation, and a 12-month period for the observations can be

assumed. For social communication networks, they always have time-varying graph structures where connections and message frequencies fluctuate periodically.

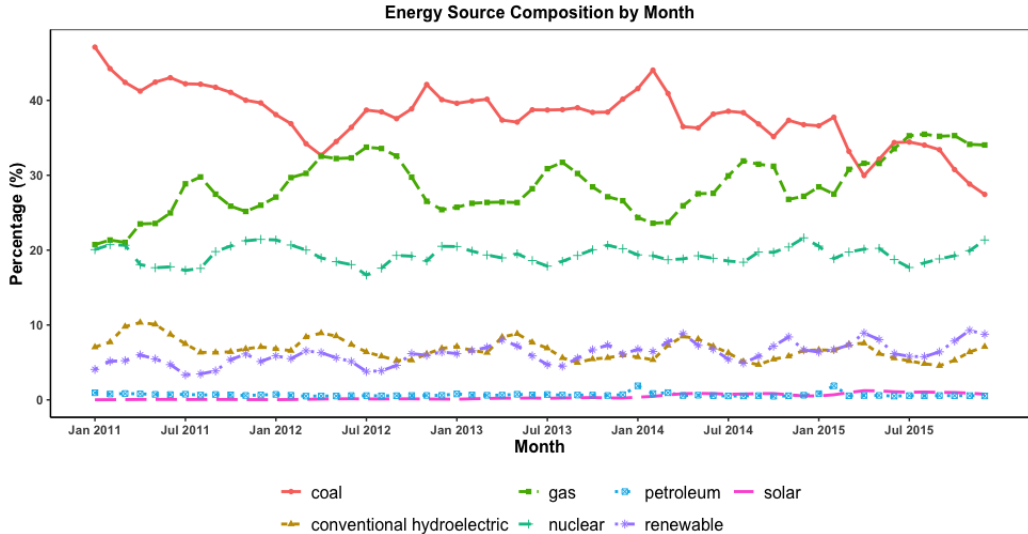


Fig. 1: The timeline of U.S. electricity generation compositions from January 2011 to December 2015. Each line represents the percentage of the corresponding energy resource categories.

All the examples above exhibit periodic behaviour, but the specific periodicity, such as the length of the period, is often an assumption rather than a certainty. For example, Figure 1 shows the timeline of U.S. electricity generation compositions from January 2011 to December 2015, considering 7 major resource categories. It is hard to directly discern a clear periodic pattern and thus there is a need for the period to be rigorously quantified using suitable statistical tools.

Notably, periodicity is a fundamental characteristic of time-varying data, and ignoring it can have negative effects. For instance, prediction intervals tend to be more precise when the periodic pattern of the data is accounted for, whereas neglecting periodicity often results in overly wide intervals. Furthermore, [Guo and Modarres \(2020\)](#) and [Xu et al. \(2025\)](#) demonstrate that neglecting periodicity can

degrade the performance of change point detection, as periodic patterns may blur the actual change points. These examples also underscore the importance of quantifying periodicity in data analysis.

So far, numerous methods on periodicity quantification have only focused on Euclidean time-varying data, such as univariate real-valued time series. These techniques fall into two broad categories: parametric approaches, which model periodic patterns using trigonometric regressions (Walker 1971; Rice and Rosenblatt 1988; Quinn and Thomson 1991), and nonparametric methods, which frame periodicity estimation as a model selection problem (Hall et al. 2000; Sun et al. 2012; Vogt and Linton 2014). However, despite a rich literature on periodicity estimation for Euclidean data, quantifying periodicity in general non-Euclidean random objects remains largely unexplored. Although the extension of trigonometric regression methods for functional data, a special case of object data, has been studied in Hörmann et al. (2018), their approach, like other parametric methods for periodic Euclidean data, relies on the linear structure of the data space and is inapplicable to general metric spaces without any local or global linear structure.

Motivated by these challenges, this paper introduces a novel nonparametric framework for periodicity quantification for time-varying random objects. Our framework consists of two main components: (i) estimation of the unknown period and (ii) quantification of the periodic component based on the estimated period. For period estimation, we adapt the idea of Vogt and Linton (2014) from Euclidean data to non-Euclidean data where we formulate the period estimation problem as one of model selection. Crucially, the absence of linear structure in general metric spaces requires significant departures from the proof techniques commonly used in nonparametric periodicity estimation (e.g., Vogt and Linton (2014) and Wang

et al. (2022)), which typically rely on an explicit additive error term structure. Moreover, we further develop information criteria for data-driven tuning parameter selection to ensure the consistency of the period estimation and provide general theoretical guidance for constructing suitable information criteria, both of which are not considered in Vogt and Linton (2014) and Wang et al. (2022), even for Euclidean data. Regarding the periodic component quantification, we leverage the Fréchet regression framework of Petersen and Müller (2019). The estimator used in the periodic component quantification is a statistic depending on the estimated period, which results in additional theoretical challenges compared to the classical Fréchet regression in Petersen and Müller (2019).

Our proposed approach represents a significant advancement in periodicity quantification for random objects. To the best of our knowledge, this is the first general framework proposed for this problem, extending beyond functional data to a wide range of non-Euclidean random objects. Extensive simulations on periodic random objects, including compositional data, networks, and functional data, showcase the superior accuracy of our method in both period estimation and periodic component quantification. We further validate its effectiveness through applications to three real-world datasets: (i) monthly U.S. electricity generation compositions, (ii) hourly transportation networks from the New York City Citi Bike system, and (iii) daily water consumption curves in Germany. In each case, our method provides interpretable and meaningful insights into the periodic structure of the data.

The remainder of this paper is organized as follows. Section 2 introduces our methodology, covering model selection and tuning parameter selection. Section 3 presents theoretical results on period estimation consistency, information criteria for

model selection, and periodic component quantification. Section 4 evaluates finite-sample performance through simulations across various types of random objects. Section 5 applies our method to three real-world datasets. Assumptions are provided in the Appendix, and all the proofs are included in the Supplementary Material.

2. Methodology

In this section, we first present the problem setup for periodic non-Euclidean random objects and then generalize the basic idea of the nonparametric period estimation method from Euclidean space to a general metric space in Section 2.1. We introduce nonparametric methodologies for period estimation, tuning parameter selection, and periodic component estimation in Sections 2.2 and 2.3.

2.1. Preliminaries

Suppose we have independent observations Y_1, \dots, Y_T of a random object within a metric space Ω with metric d and that the observations have a periodic pattern with the true smallest period being a positive integer θ_0 . For generic probability measures $P^{(l)}$ on (Ω, d) with $l \in \{1, \dots, \theta_0\}$, consider the product measures $P^{\theta_0} = P^{(1)} \times \dots \times P^{(\theta_0)}$. Then $\{Y_t\}_{t=1}^T$ is said to follow a θ_0 -periodic distribution P^{θ_0} if there exists a positive integer θ_0 such that, for any integer $j \in \{1, \dots, \theta_0\}$, (i) $Y_j \sim P^{(j)}$ and (ii) $Y_j, Y_{j+\theta_0}, Y_{j+2\theta_0}, \dots, Y_{j+k\theta_0}$ have the same distribution for integer $k \geq 0$ satisfying $j + k\theta_0 \leq T$.

For periodic random objects Y_1, \dots, Y_T following the distribution P^{θ_0} , the corresponding population Fréchet mean (Fréchet 1948) can be defined by

$$m(r(t, \theta_0)) = \arg \min_{\omega \in \Omega} \mathbb{E}\{d^2(Y_t, \omega)\}, \quad (1)$$

where $r(t, \theta_0) = t + \theta_0 - \theta_0 \lfloor (t + \theta_0 - 1)/\theta_0 \rfloor$ with $\lfloor \cdot \rfloor$ being the floor function, and $m(\cdot) \in \Omega$ is the deterministic periodic component with period θ_0 and domain being the set of positive integers such that $m(l) = m(l + \theta_0) = m(l + 2\theta_0) = \dots$ for $l \in \{1, 2, \dots, \theta_0\}$.

In this framework, we do not assume any specific parametric structure of the periodic component $m(\cdot)$, and $m(\cdot)$ is treated as a sequence rather than a Ω -valued function. Our main focus is the equidistant design which is the most common situation, as seen in the real data examples considered.

We now consider a special case where the metric space $\Omega = \mathbb{R}$ with the metric d_E being the Euclidean distance. Thanks to the linear structure of the Euclidean space \mathbb{R} , one can further assume that the observations Y_1, \dots, Y_T satisfying (1) follows the model

$$Y_t = m_E(t) + \epsilon_t \quad (t = 1, \dots, T), \quad (2)$$

where the random noise ϵ_t is independent with mean $\mathbb{E}(\epsilon_t) = 0$, $m_E(t) = m(t)$ in (1) and the subscript E in $m_E(\cdot)$ indicates that $m_E(\cdot)$ is in the Euclidean space \mathbb{R} . Construct β and \mathbf{x}_t depending on the value of θ as $\beta = \beta(\theta) = (m_E(1), \dots, m_E(\theta))^\top$ and $\mathbf{x}_t = \mathbf{x}_t(\theta) = (x_{t1}, \dots, x_{t\theta})^\top$ where $x_{tj} = 1$ for $j = t + \theta - \theta \lfloor (t + \theta - 1)/\theta \rfloor$ and $x_{tk} = 0$ for $k \neq j$. Then the model (2) can be rewritten as

$$Y_t = \mathbf{x}_t^\top \beta + \epsilon_t \quad (t = 1, \dots, T), \quad (3)$$

when $\theta = \theta_0$ in β and \mathbf{x}_t . The ordinary least-square (OLS) estimate of β is then given by $\hat{\beta} = (X^\top X)^{-1} X^\top \mathbf{Y}$, where $X = X(\theta_0) = (\mathbf{x}_1, \dots, \mathbf{x}_T)^\top$ and $\mathbf{Y} = (Y_1, \dots, Y_T)^\top$.

To estimate the period θ_0 , [Vogt and Linton \(2014\)](#) consider transforming the period estimation problem into a model selection problem, by first obtaining $\hat{\beta}$ for each candidate period $\theta \in \{1, 2, \dots, \Theta_T\}$, where Θ_T is the upper bound of the candidates, then calculating the Euclidean model fitting measure as $\text{RSS}_E = \|\mathbf{Y} - X\hat{\beta}\|_E^2$ and evaluating the penalized RSS_E as $\mathcal{L}(\theta, \lambda_T) = \|\mathbf{Y} - X\hat{\beta}\|_E^2 + \lambda_T\theta$ for a tuning parameter λ_T . Here, $\|\cdot\|_E$ denotes the Euclidean norm and the tuning parameter λ_T diverges to infinity at an appropriate rate (see [Vogt and Linton \(2014\)](#)). The estimator $\hat{\theta}_{\lambda_T}$ of the true period θ_0 is obtained by

$$\hat{\theta}_{\lambda_T} = \arg \min_{1 \leq \theta \leq \Theta_T} \mathcal{L}(\theta, \lambda_T).$$

However, the method considered in [Vogt and Linton \(2014\)](#) has two main limitations. The first is that either the model in the form of (3) or the OLS estimate of β depends on the linearity property, posing significant challenges in a direct extension of this method to deal with non-Euclidean random objects. The second limitation is that [Vogt and Linton \(2014\)](#) do not offer any theoretical justification for selecting tuning parameters in a data-driven manner.

Here we address the first limitation, while the second limitation is dealt with in the next section. Inspired by the Fréchet regression proposed by [Petersen and Müller \(2019\)](#), we first observe that the Euclidean model fitting measure $\text{RSS}_E = \sum_{t=1}^T d_E^2(Y_t, \hat{Y}_t)$ where \hat{Y}_t is the fitted value using the OLS estimator $\hat{\beta}$ and thus

$$\hat{Y}_t = \mathbf{x}_t^\top \hat{\beta} = \mathbf{x}_t^\top (X^\top X)^{-1} X^\top \mathbf{Y} = \arg \min_{z \in \mathbb{R}} T^{-1} \sum_{i=1}^T s_i^{(t)} d_E^2(Y_i, z),$$

where $\mathbf{s}^{(t)} = (s_1^{(t)}, \dots, s_T^{(t)}) = \mathbf{x}_t^\top (X^\top X)^{-1} X^\top$. This means the Euclidean model fitting measure RSS_E measures the summation, over $t = 1, \dots, T$, of the squared Euclidean distance between each observation and a corresponding point which is the weighted barycentre of all the observations. This key finding enables us to generalize the period estimation problem in Euclidean space to a general metric space without requiring any linear structures, as given in the next section.

2.2. Period Estimation for Random Objects

For a given θ , construct \mathbf{x}_t and X as defined below (2) and (3), respectively. To calculate the required weighted barycenter, we first build a global Fréchet regression model as

$$m_{F,t}(\theta, T) = \arg \min_{\omega \in \Omega} M_{F,t}(\omega; \theta, T), \quad M_{F,t}(\omega; \theta, T) = T^{-1} \sum_{i=1}^T s_i^{(t)} \mathbb{E} [d^2(Y_i, \omega)], \quad (4)$$

for $t = 1, \dots, T$ where $s_i^{(t)}$ is defined to be the i -th column of $\mathbf{x}_t^\top (X^\top X)^{-1} X^\top$. Note that once θ and T are specified, \mathbf{x}_t and X are also fully specified. Consequently, the weights $\{s_i^{(t)}\}_{i=1}^T$ in the cost function $M_{F,t}(\omega; \theta, T)$ depend only on θ and T . Moreover, based on the construction of \mathbf{x}_t and X , $s_i^{(t)}$ is fixed rather than random as in Petersen and Müller (2019). Moreover, as $\{Y_t\}_{t=1}^T$ follow a θ_0 -periodic distribution P^{θ_0} , Y_1, \dots, Y_T are not identically distributed whereas Petersen and Müller (2019) require an identically distributed assumption. By Lemma S1 in the Supplementary Material, one can see that $m_{F,t}(\theta, T) = m(r(t, \theta_0))$ defined in (1) when $\theta = \theta_0$.

The estimator of $m_{F,t}(\theta, T)$, $t = 1, \dots, T$, is then given by

$$\hat{m}_{F,t}(\theta, T) = \arg \min_{\omega \in \Omega} \hat{M}_{F,t}(\omega; \theta, T), \quad \hat{M}_{F,t}(\omega; \theta, T) = T^{-1} \sum_{i=1}^T s_i^{(t)} d^2(Y_i, \omega).$$

Let Θ_T be an upper bound of the scanning candidates and for each candidate period $\theta \in \{1, 2, \dots, \Theta_T\}$, calculate $\{\hat{m}_{F,t}(\theta, T)\}_{t=1,\dots,T}$ and evaluate the penalized residual sum of squares (RSS) as

$$\mathcal{L}(\theta, \lambda_T) = \text{RSS}(\theta) + \lambda_T \theta, \quad (5)$$

where $\text{RSS}(\theta) = \sum_{t=1}^T d^2(Y_t, \hat{m}_{F,t}(\theta, T))$ is a goodness-of-fit measure generalizing the Euclidean model fitting measure RSS_E defined in Section 2.1, and the tuning parameter λ_T diverges to infinity at an appropriate rate; see Theorem 1 below in Section 3. The estimator of the true period θ_0 , denoted as $\hat{\theta}_{\lambda_T}$, is

$$\hat{\theta}_{\lambda_T} = \arg \min_{1 \leq \theta \leq \Theta_T} \mathcal{L}(\theta, \lambda_T). \quad (6)$$

Here, the upper bound Θ_T is allowed to grow with the sample size T at a suitable rate, see Theorem 1. Although we do not have the coefficient parameter in the global Fréchet regression, the penalty term $\lambda_T \theta$ in (5) can be viewed as an ℓ_0 -penalty as θ can be interpreted as the number of model parameters as θ controls the dimension of the covariate vectors. The period estimation problem is now formulated as a model selection problem where for each candidate $\theta \in \{1, \dots, \Theta_T\}$, we construct a model of the form (4). The goal is then to identify the correct model among these candidates.

There is a rich body of literature on ℓ_0 -penalized model selection for Euclidean data (see e.g., [Claeskens and Hjort \(2008\)](#)). However, little work has been done on model selection or variable selection in the context of Fréchet regressions. The most relevant study is [Tucker et al. \(2023\)](#) which focuses on ℓ_2 -penalties and is therefore not applicable to our setting. Moreover, the proposed ℓ_0 -penalized method achieves

computational efficiency by evaluating the penalized RSS $\mathcal{L}(\theta, \lambda_T)$ for Θ_T different choices of θ .

Notably, the visualization of random objects remains an underdeveloped area in the literature, and no existing visualization tool effectively reveals the presence of periodicity in random objects. Our proposed penalized RSS in (5) provides a powerful tool to address this gap. For example, in Figure 2(a), consider the U.S. electricity generation compositions from January 2011 to December 2015, a pronounced drop in the penalized RSS at a specific value, together with drops at its positive integer multiples, strongly suggests the presence of a periodic pattern in the object data. Figure 2(a) indicates that the U.S. electricity generation compositions have a period of 12 while the periodic pattern cannot be directly observed in the line plot of each elements of the compositions as shown in Figure 1.

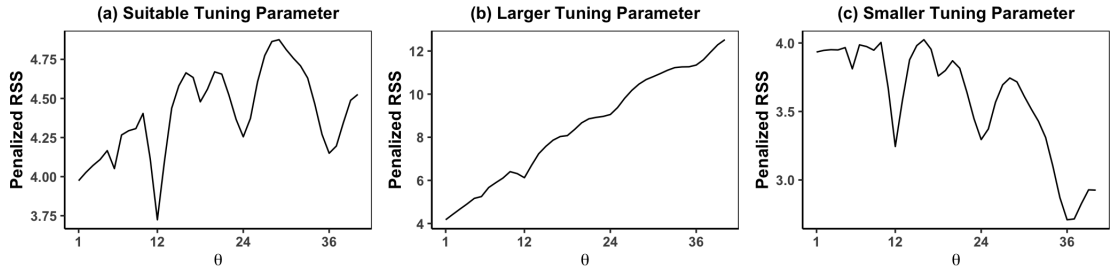


Fig. 2: Plots of the penalized RSS for U.S. electricity generation compositions from January 2011 to December 2015 considering different choice of the tuning parameter. In particular, a suitable choice of $\lambda_T = \hat{\lambda}$ with $\hat{\lambda}$ selected via (8)

in (a), $\lambda_T = 5\hat{\lambda}$ in (b), and $\lambda_T = \hat{\lambda}/5$ in (c).

In (5), the tuning parameter λ_T plays a crucial role in estimation. As one can see in Figures 2(b) and 2(c), a tuning parameter that is too small can lead to overfitting, while one that is too large can cause misspecification, resulting in inaccurate estimation of the true period θ_0 . Motivated by the Bayesian information

criterion (Schwarz 1978), we develop a data-driven information criterion for selecting the tuning parameter. Notably, existing nonparametric methods for Euclidean data, such as those proposed by Vogt and Linton (2014) and Wang et al. (2022), do not incorporate a data-driven approach for tuning parameter selection. This constitutes one of the contributions of our work.

Here, we consider a general regularization function $g(T)$, such that an information criterion of the form

$$\text{IC}_\lambda = \log\{\text{RSS}(\hat{\theta}_\lambda)/T\} + \hat{\theta}_\lambda g(T), \text{ or } \text{IC}_\lambda = \text{RSS}(\hat{\theta}_\lambda)/T + \hat{\theta}_\lambda g(T), \quad (7)$$

can consistently estimate the true period θ_0 . We aim to develop a general theoretical framework for the information criterion (7) and the conditions for constructing the general regularization function $g(T)$ in (7) are given in Theorem 2 below. An analogous framework can be found in the area of factor models; see, e.g. Bai and Ng (2002). Using (7), the tuning parameter λ may be selected as

$$\hat{\lambda} = \arg \min_{\lambda} \text{IC}_\lambda. \quad (8)$$

Based on the information criteria in (8), the final period estimator is given by $\hat{\theta}_{\hat{\lambda}}$, obtained from (6) by setting $\lambda_T = \hat{\lambda}$.

2.3. Periodic Component Estimation for Random Objects

Write $\hat{\theta}_{\hat{\lambda}}$ for the estimator of the true but unknown period θ_0 . Let \mathbb{N}^+ be the set of positive integers. Then an estimator of the periodic sequence $\{m(t)\}_{t \in \mathbb{N}^+}$ given by

(1) is

$$\hat{m}(l) = \hat{m}_{F,l} \left(\hat{\theta}_{\hat{\lambda}}, T \right), \quad (9)$$

and $\hat{m}(l + k\hat{\theta}_{\hat{\lambda}}) = \hat{m}(l)$ for $l = 1, 2, \dots, \hat{\theta}_{\hat{\lambda}}$ and all $k = 0, 1, 2, \dots$. It is worth noting that by our construction, we always have $\hat{m}_{F,l+k\hat{\theta}_{\hat{\lambda}}} \left(\hat{\theta}_{\hat{\lambda}}, T \right) = \hat{m}_{F,l} \left(\hat{\theta}_{\hat{\lambda}}, T \right)$ for $l = 1, 2, \dots, \hat{\theta}_{\hat{\lambda}}$ and all $k = 0, 1, 2, \dots$. Therefore, by construction, $\{\hat{m}(t)\}_{t=1,\dots,T}$ is a periodic sequence with period $\hat{\theta}_{\hat{\lambda}}$.

Although the periodic component estimation in (9) looks similar to the empirical version of the global Fréchet regression in Petersen and Müller (2019), one should notice that the periodic component estimator is actually a statistic with the additional estimated parameter, $\hat{\theta}_{\hat{\lambda}}$. This will pose some challenges in establishing theoretical results as this additional estimated parameter involves additional randomness. To deal with the statistic with estimated parameters, the classical way and the method adopted in the proof is to first introduce an oracle estimator $\tilde{m}(l)$ in the case where the true period θ_0 is assumed to be known. We then evaluate the asymptotic behaviours of $d(\hat{m}(l), \tilde{m}(l))$ and $d(\tilde{m}(l), m(l))$, respectively.

3. Theoretical Results

3.1. Theoretical Results for the Period Estimator and Tuning Parameter Selection

Theorem 1 given below characterizes the asymptotic behaviour of the period estimator $\hat{\theta}_{\lambda}$ given by (6). To concisely express the requirement for the tuning parameter, denote $a_T \ll b_T$ or $b_T \gg a_T$ as $a_T = o(b_T)$ for any two sequences $\{a_T\}$ and $\{b_T\}$.

Theorem 1 Suppose $\Theta_T = \Theta$ is fixed. Then under Assumptions A1-A3 in the Appendix, with the tuning parameter λ_T selected such that $T^{1-1/(\beta_1-1)} \ll \lambda_T \ll T$ where β_1 is given in Assumption A3 and reflects the local curvature of the Fréchet squared loss function $M_{F,t}(\omega; \theta, T)$ near its minimum, we have

$$\hat{\theta}_{\lambda_T} = \theta_0 + o_p(1)$$

as $T \rightarrow \infty$. Furthermore, assume that $\Theta_T \rightarrow \infty$ and $\Theta_T/T \rightarrow 0$ as $T \rightarrow \infty$. Select the tuning parameter λ_T such that $T^{1-1/(\beta'_2-1)}\Theta_T^{1/(\beta'_2-1)} \ll \lambda_T \ll T$ for any $\beta'_2 > \beta_2$ where β_2 is given in Assumption A6 and reflects the uniform local curvature of the Fréchet squared loss function $M_{F,t}(\omega; \theta, T)$ near its minimum over $\theta \in \{1, 2, \dots, \Theta_T\}$. Then $\hat{\theta}_{\lambda_T} = \theta_0 + o_p(1)$ as $T \rightarrow \infty$ under Assumptions A1-A6 in the Appendix.

Remark 1 Theorem 1 is developed by analysing $\mathcal{L}(\theta)$ in two sets $\mathcal{M}_1 = \{\theta : \theta = k\theta_0, k = 2, \dots, \text{ and } 1 \leq \theta \leq \Theta_T\}$ and $\mathcal{M}_2 = \{\theta : \theta \neq \theta_0, \theta \notin \mathcal{M}_1, \text{ and } 1 \leq \theta \leq \Theta_T\}$. \mathcal{M}_1 corresponds to the overfitting situation while \mathcal{M}_2 can be interpreted as the misspecification case. When $\Theta_T = \Theta$ is fixed, both sets \mathcal{M}_1 and \mathcal{M}_2 have finite cardinality and an asymptotic result for $\hat{m}_{F,t}(\theta, T)$ for every fixed θ is sufficient. When $\Theta_T \rightarrow \infty$, the cardinality of either \mathcal{M}_1 or \mathcal{M}_2 is not finite any more, resulting in the need for stronger assumptions to achieve the uniform result for $\hat{m}_{F,t}(\theta, T)$ over $\theta \in \{1, 2, \dots, \Theta_T\}$. See the proof of Theorem 1 in the Supplementary Material for details. A discussion of a similar situation in tuning parameter selection can be found in Section 2.2 of Wang et al. (2009).

Remark 2 Metric spaces that satisfy Assumption A3 with $\beta_1 = 2$ and Assumption Assumption A6 with $\beta_2 = 2$ include symmetric positive definite matrices of fixed dimensions with the Frobenius metric, graph Laplacian matrices with the Frobenius metric, univariate probability distributions with the 2-Wasserstein metric, and the unit sphere with the geodesic distance metric (see Petersen and Müller (2019) and Dubey and Müller (2021)).

Theorem 1 establishes the consistency result of the proposed period estimator $\hat{\theta}_{\lambda_T}$ under a broad class of tuning sequences of λ_T . Specifically, the result holds for all λ_T satisfying $T^{1-1/(\beta_1-1)} \ll \lambda_T \ll T$ when $\Theta_T = \Theta$ is fixed or $T^{1-1/(\beta_2'-1)}\Theta_T^{1/(\beta_2'-1)} \ll \lambda_T \ll T$. This flexible range accommodates a variety of growth rates for the tuning parameter λ_T . This means, selecting any λ_T satisfying this flexible range of condition can lead to estimation consistency asymptotically. However, for a given real dataset, the performance of $\hat{\theta}_{\lambda_T}$ can be sensitive to λ_T selected from this range, as seen in Figure 2 earlier. Hence, using this range only to select λ_T is not practical. To this end, we provide a data-driven approach to select the tuning λ_T , and we theoretically show that using the data-driven approach to select λ_T can also leads to selection consistency. It is seen in Sections 4, 5 and Section S3 in the Supplementary Material that it provides reliable performance of period estimation for different finite settings in numerical studies.

To establish the theory of the information criterion, we partition λ into three mutually exclusive sets $\Lambda_0 = \{\lambda : \hat{\theta}_\lambda = \theta_0\}$, $\Lambda_+ = \{\lambda : \hat{\theta}_\lambda \in \mathcal{M}_{\theta_0}, \hat{\theta}_\lambda \neq \theta_0\}$ and $\Lambda_- = \{\lambda : \hat{\theta}_\lambda \notin \mathcal{M}_{\theta_0}\}$, where $\mathcal{M}_{\theta_0} = \{\theta : \theta = k\theta_0, k = 1, 2, \dots, 1 \leq \theta \leq \Theta_T\}$. One can see that the sets Λ_0 , Λ_+ and Λ_- correspond to whether the resulting global Fréchet regression estimator $\hat{m}_F(\cdot)$ is correctly fitted, overfitted or misspecified.

Theorem 2 Suppose $\Theta_T = \Theta$ is fixed. Then under Assumptions A1-A3,

$$\mathbb{P} \left(\min_{\lambda \in \Lambda_+ \cup \Lambda_-} \text{IC}_\lambda > \text{IC}_{\lambda_T} \right) \rightarrow 1 \quad (10)$$

holds as $T \rightarrow \infty$ if (i) $g(T) \gg T^{-1/(\beta_1-1)}$ and (ii) $g(T) = o(1)$ as $T \rightarrow \infty$ for any reference tuning parameter λ_T satisfying $T^{1-1/(\beta_1-1)} \ll \lambda_T \ll T$ where β_1 is given in Assumption A3. Furthermore, assume that $\Theta_T \rightarrow \infty$ and $\Theta_T/T \rightarrow 0$ as $T \rightarrow \infty$. Then under Assumptions A1-A6, (10) holds as $T \rightarrow \infty$ if (iii) $g(T) \gg (T/\Theta_T)^{-1/(\beta'_2-1)}$ and (iv) $g(T) = o(1)$ as $T \rightarrow \infty$ for any reference tuning parameter λ_T satisfying $T^{1-1/(\beta'_2-1)} \Theta_T^{1/(\beta'_2-1)} \ll \lambda_T \ll T$, for any $\beta'_2 > \beta_2$, with β_2 given in Assumption A6.

Remark 3 When $\Theta_T = \Theta$ is fixed, the set $\lambda \in \Lambda_+ \cup \Lambda_-$ has finite cardinality and it is sufficient to show $\mathbb{P}(\text{IC}_\lambda > \text{IC}_{\lambda_T}) \rightarrow 1$ for every $\lambda \in \Lambda_+ \cup \Lambda_-$. When $\Theta_T \rightarrow \infty$, the cardinality of $\lambda \in \Lambda_+ \cup \Lambda_-$ is not finite and $\mathbb{P}(\text{IC}_\lambda > \text{IC}_{\lambda_T}) \rightarrow 1$ cannot imply $\mathbb{P}(\min_{\lambda \in \Lambda_+ \cup \Lambda_-} \text{IC}_\lambda > \text{IC}_{\lambda_T}) \rightarrow 1$. Thus stronger assumptions are needed to achieve the uniform result for $\hat{m}_{F,t}(\theta, T)$ over $\theta \in \{1, 2, \dots, \Theta_T\}$.

Theorem 2 indicates that any λ failing to identify the true period cannot be selected as the optimal tuning parameter. To see this, note that by Theorem 1, we have $\hat{\theta}_{\lambda_T} = \theta_0 + o_p(1)$ as $T \rightarrow \infty$ when λ_T satisfying the condition in Theorem 1. Therefore, Theorem 2 indicates that if λ falls into the set Λ_+ or Λ_- , then the corresponding IC_λ will be larger than the reference level IC_{λ_T} with probability tending to 1 as $T \rightarrow \infty$. For $\hat{\lambda} = \arg \min_\lambda \text{IC}_\lambda$, we always have $\text{IC}_{\hat{\lambda}} \leq \text{IC}_{\lambda_T}$, which can ensure that $\hat{\lambda}$ falls into the set $\Lambda_0 = \{\lambda : \hat{\theta}_\lambda = \theta_0\}$.

Moreover, as we allow $\Theta_T \rightarrow \infty$ as $T \rightarrow \infty$, this means the range of the candidate models diverges and it is not surprising that the regularization function $g(T)$ involves Θ_T , see, e.g., [Chen and Chen \(2008\)](#) and [Zhang \(2025\)](#). When $\Theta_T = \Theta$ is fixed and for metric spaces that satisfy $\beta_1 = 2$ given in Assumption [A3](#), see Remark 1, Theorem 2 leads to a specific consideration of the information criterion which is the classical Bayesian information criterion ([Schwarz 1978](#)) as $\text{BIC}_\lambda = \log\{\text{RSS}(\hat{\theta}_\lambda)/T\} + \hat{\theta}_\lambda \log(T)/T$.

Combining Theorem 1 and Theorem 2 establishes the consistency of $\hat{\theta}_{\hat{\lambda}}$ with $\hat{\lambda}$ selected via (8), shown in Corollary 3 below.

Corollary 3 *Suppose the conditions in Theorem 2 hold. Then $\hat{\theta}_{\hat{\lambda}} - \theta_0 = o_p(1)$ with $\hat{\lambda}$ given by (8).*

3.2. Theoretical Result for the Periodic Component Estimator

We now establish the convergence rate of the periodic component estimator $\hat{m}(t)$ for $t = 1, \dots, T$ given by (9).

Theorem 4 *Under Assumptions [A1-A6](#) in the Appendix,*

$$\max_{t=1,\dots,T} d(\hat{m}(t), m(t)) = O_p\left(T^{-1/2(\beta_1-1)}\right).$$

Theorem 4 presents a uniform convergence result with only the required assumption for pointwise convergence results such that $d(\tilde{m}(t), m(t)) = O_p\left(T^{-1/2(\beta_1-1)}\right)$ holds for every $t = 1, \dots, T$. This is because the maximum over $1, \dots, T$ is the same as over $1, \dots, \hat{\theta}_{\hat{\lambda}}$ while we have $\hat{\theta}_{\hat{\lambda}} = \theta_0$ with probability tending to 1 as $T \rightarrow \infty$ by Theorem 1 and Theorem 2.

4. Simulation Studies

In this section, we illustrate our method by the simulation of periodic compositional data. Additional simulation results for networks and functional data can be found in Sections S3.1 and S3.2 in the Supplementary Material. For each scenario, we replicate the simulation 200 times with sample size T varying in $\{100, 240, 500\}$ and with three different levels of noise. The tuning parameter λ_T is chosen by minimizing the information criterion in (7), with the regularization function $g(T)$ taking the form of $\log(T/\Theta_T)/(T/\Theta_T)^{1.01}$, where Θ_T is allowed to grow with the sample size T . Note that this choice of $g(T)$ satisfies the conditions in Theorem 2.

4.1. Periodic Composition Generation

The generation of a periodic composition is based on the Dirichlet distribution which is a multivariate generalization of the beta distribution; see e.g. page 44 of [Mardia et al \(1979\)](#). Each simulated Y_t takes values a two-simplex $\Delta^2 = \{\boldsymbol{\delta} = (\delta_1, \delta_2, \delta_3)^\top \in \mathbb{R}^3 : \sum_{l=1}^3 \delta_l = 1 \text{ and } \delta_p > 0 \text{ for } p = 1, 2, 3\}$. Defining

$$l_t = \sin \left(0.1 + \frac{r(t-1, \theta_0)}{11} (\pi - 0.2) \right)$$

with the true period $\theta_0 = 12$, Y_t is sampled independently from the Dirichlet distribution $\text{Dir}(\boldsymbol{\alpha})$, where $\boldsymbol{\alpha} = (l_t \alpha, l_t \alpha, \alpha)^\top$. Note that l_t controls the mean of each element of Y_t , while l_t and α control the variance of each element of Y_t . Additionally, when α becomes smaller, the variance becomes larger.

Figure 3 clearly exhibits periodic behaviour, where the simulated compositions transition from being highly concentrated along the boundary of the simplex to more evenly distributed across the simplex, before returning to a concentrated state along the boundary.

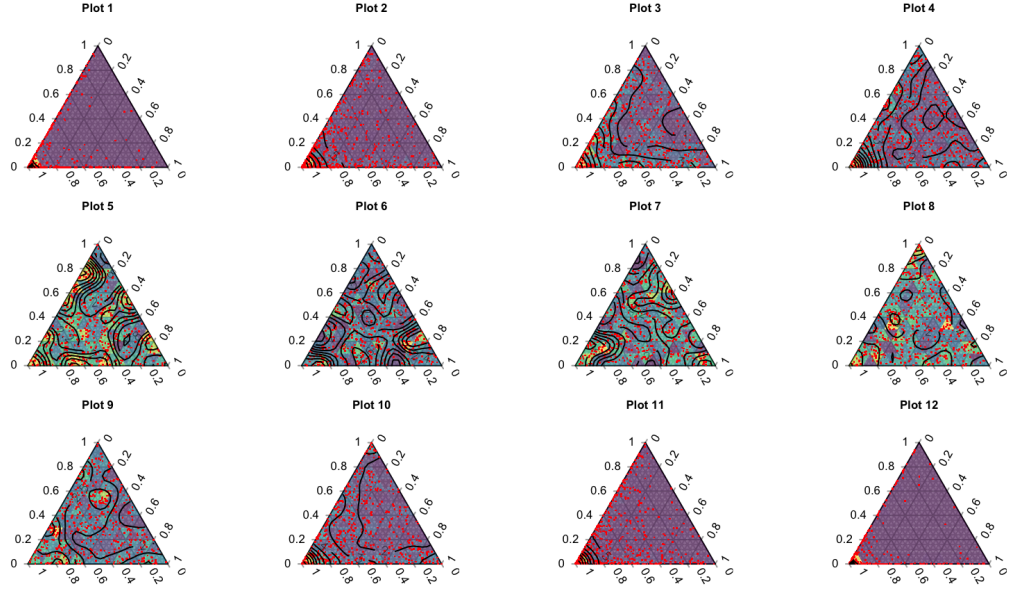


Fig. 3: Ternary plots of generated periodic compositions with densities for the period being 12.

4.2. Simulation Results

In this simulation, we consider the square root transformation for compositional data (Scealy and Welsh 2011), resulting in spherical data, and choose the corresponding metric be the geodesic distance; that is, we use the metric given by

$$d_S(\mathbf{s}_1, \mathbf{s}_2) = \arccos(\mathbf{s}_1^\top \mathbf{s}_2)$$

where $\mathbf{s}_i = \sqrt{\boldsymbol{\delta}_i}$ for $i = 1, 2$ with $\boldsymbol{\delta}_i$ being a compositional data vector and $\sqrt{\cdot}$ being the positive component-wise square root. To fit a global Fréchet regression for spherical data, we follow the techniques proposed by Petersen and Müller (2019), and the range of the period candidates is set to grow at the rate of \sqrt{T} . When $T = 100$, $\Theta_T = 40$ which covers three full periods, since the true period is 12 and $3 \times 12 < \Theta_T = 40$. When $T = 240$, $\Theta_T = 62$, while when $T = 500$, Θ_T is set to be

89. Denote $p(\hat{\theta}_{\lambda} = a)$ as the proportion of cases where $\hat{\theta}_{\lambda} = a$ across 200 replicates, and $p(b \leq \hat{\theta}_{\lambda} \leq c)$ as the proportion of cases where $b \leq \hat{\theta}_{\lambda} \leq c$ across 200 replicates, for some integers a, b and c .

Table 1. Empirical probabilities that $\hat{\theta}_{\lambda} = 12$, reported in the first three columns, and that $8 \leq \hat{\theta}_{\lambda} \leq 16$, reported in the last three columns, for the sample size T varies in $\{100, 240, 500\}$ and different levels of element-wise variance of each observation when the simulated samples are periodic compositions and the information criterion is for the logarithm of residual sum of squares.

	$p(\hat{\theta}_{\lambda} = 12)$			$p(8 \leq \hat{\theta}_{\lambda} \leq 16)$		
	$T = 100$	$T = 240$	$T = 500$	$T = 100$	$T = 240$	$T = 500$
$\alpha = 1$	0.865	0.995	1.000	0.865	0.995	1.000
$\alpha = 0.5$	0.715	0.975	0.990	0.725	0.975	0.990
$\alpha = 0.1$	0.150	0.825	0.845	0.175	0.825	0.845

Table 1 presents the simulation results for periodic compositions using the first IC in (7). The first three columns of the table report the probabilities that the estimator $\hat{\theta}_{\lambda}$ correctly identifies the true period $\theta_0 = 12$, while the last three columns of the table show the probabilities of $\hat{\theta}_{\lambda}$ ranging from 8 to 16. Notably, our proposed estimator exhibits high accuracy even with a small sample size when the variance of each element of Y_t is small. When the variance becomes large, it is not surprising that the finite sample performance of the estimator becomes worse for small sample sizes. Nonetheless, the estimator typically provides a good approximation of the true period in most cases. Its accuracy increases rapidly with the number of observed cycles of the periodic pattern.

Table 2. Empirical probabilities that $\hat{\theta}_{\lambda} = 12$, reported in the first three columns, and that $8 \leq \hat{\theta}_{\lambda} \leq 16$, reported in the last three columns, for the sample size T varies in $\{100, 240, 500\}$ and different levels of element-wise variance of each observation when the simulated samples are periodic compositions and the information criterion is for the residual sum of squares.

	$p(\hat{\theta}_{\lambda} = 12)$			$p(8 \leq \hat{\theta}_{\lambda} \leq 16)$		
	$T = 100$	$T = 240$	$T = 500$	$T = 100$	$T = 240$	$T = 500$
$\alpha = 1$	0.930	1.000	1.000	0.930	1.000	1.000
$\alpha = 0.5$	0.805	0.995	1.000	0.815	0.995	1.000
$\alpha = 0.1$	0.535	0.825	0.890	0.640	0.825	0.890

Table 2 provides the simulation results for periodic compositions using the second IC in (7). The results exhibit patterns similar to those in Table 1. Importantly, the second IC in (7) yields slightly improved finite-sample performance relative to the first IC, with the improvement being most pronounced for smaller sample sizes T . When the sample size $T = 500$, the estimator always hits the value of the true period even when the variance of each element of Y_t is larger such as $\alpha = 0.5$.

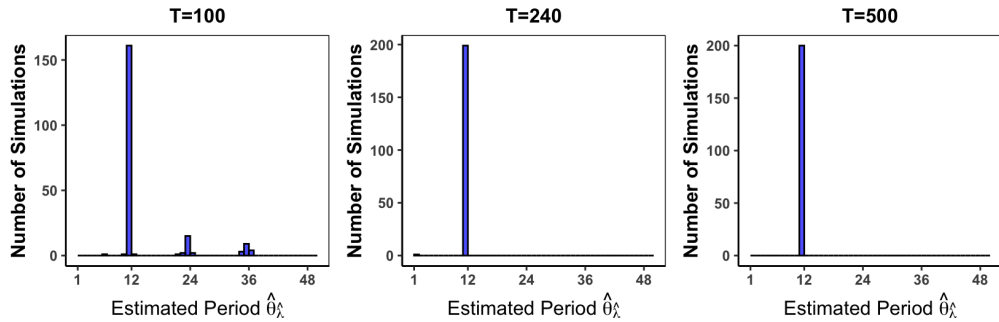


Fig. 4: Histograms of the simulation results for periodic compositions when $\alpha = 0.5$ for different samples sizes $T \in \{100, 240, 500\}$. The bars present how many times each value of $\hat{\theta}_{\lambda}$ is observed across 200 simulation runs using the information criterion for the residual sum of squares.

Histograms of the simulation results when $\alpha = 0.5$ using the second IC in (7) for different sample sizes $T \in \{100, 240, 500\}$ are given in Figure 4. Each panel presents the distribution of $\hat{\theta}_{\lambda}$ for $T = 100, 240, 500$. The figure reveals that for a small sample size $T = 100$, alongside a primary concentration of estimates around the true period θ_0 , secondary clusters emerge around multiples of θ_0 . Although Table 2 suggests that the estimator may not always precisely recover the true period when variances are large, it still provides reasonable approximations, particularly capturing its multiples. As suggested by the proof of Theorem 1, this pattern aligns with the asymptotic behaviour of $\hat{\theta}_{\lambda}$. When the sample size increases, the clusters

around the multiples of θ_0 disappear, leading to more accurate period identification. When the sample size $T = 500$, the proposed estimator always correctly identifies the value of the true period.

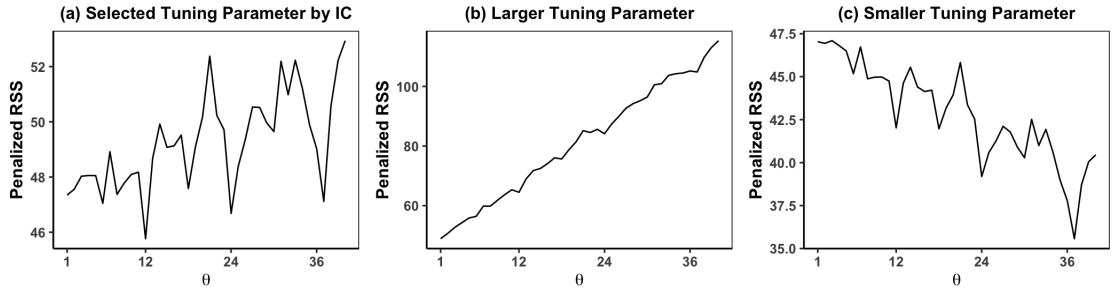


Fig. 5: Plots of penalized RSS for one simulation replicate for periodic compositions with $T = 100$ and $\alpha = 1$, considering different choices of the tuning parameter λ_T such as $\lambda_T = \hat{\lambda}$ in (a), $\lambda_T = 5\hat{\lambda}$ in (b), and $\lambda_T = \hat{\lambda}/5$ in (c), using the information criterion for the residual sum of squares.

Now we study the performance of our selected tuning parameter based on the proposed IC in (7). We conduct a typical simulation for periodic compositions with $T = 100$ and $\alpha = 1$. Figure 5 presents the penalized RSS $\mathcal{L}(\theta, \lambda_T)$ from (5) for three selected values of tuning parameter λ_T where $\lambda_T = \hat{\lambda}$ in panel (a), $\lambda_T = 5\hat{\lambda}$ in panel (b) and $\lambda_T = \hat{\lambda}/5$ in panel (c). Panels (a) and (c) in Figure 5 show that sharp decreases in the penalized RSS are observed near the true value of the period $\theta_0 = 12$ and its multiples, when the tuning parameter is not too large. Moreover, the choice of λ_T significantly affects the function's overall trend where a larger tuning parameter forces the global minimum to be 1 in panel (b) while a smaller tuning parameter causes that the global minimum occurs at a later spike instead of at the true period. These findings support the conclusion that our selected tuning parameter based on the proposed IC performs in a reasonable manner.

The final step of our proposed methodology is the estimation of the periodic component $m(t)$ of the random object, given the period estimation. Note that when Y_t is sampled independently from the Dirichlet distribution $\text{Dir}(\boldsymbol{\alpha})$ with $\boldsymbol{\alpha} = (l_t\alpha, l_t\alpha, \alpha)^\top$, then $m(t) = (l_t/(2l_t + 1), l_t/(2l_t + 1), 1/(2l_t + 1))^\top$. We denote by $\hat{m}^{(k)}(t)$ the estimated component for the k -th replicate and we calculate the mean of squared distance (MSE) for the k -th replicate between $\hat{m}^{(k)}(t)$ and $m(t)$, denoted as MSE_k , where the distance is measured by the geodesic distance after the square root transformation. The final MSE is computed as $200^{-1} \sum_{k=1}^{200} \text{MSE}_k$.

Table 3. Mean squared errors (MSEs) for periodic component estimation considering different sample sizes $T \in \{100, 240, 500\}$ and different levels of element-wise variance of each observation when the simulated samples are periodic compositions.

	$\alpha = 1$	$\alpha = 0.5$	$\alpha = 0.1$
$T = 100$	0.155	0.215	0.361
$T = 240$	0.112	0.147	0.229
$T = 500$	0.089	0.118	0.183

Table 3 shows the MSE of the periodic component estimation considering different sample sizes $T \in \{100, 240, 500\}$ and different choices of α , corresponding to the different levels of element-wise variance of each observation. For each choice of α , one can see that when the sample size increases, the MSE becomes smaller. Notably, for small sample size $T = 100$, the period estimation does not hit the true period all the time, resulting in a larger MSE. For larger sample sizes $T \in \{240, 500\}$, the period estimation accurately reach the true period, and thus gives smaller MSE. When α becomes smaller, the element-wise variance of each observation gets larger and one can observe that the MSE becomes larger for the same sample size.

Table 3 supports the finding that the finite sample performance of the periodic component estimator $\hat{m}(t)$ for $t = 1, \dots, T$ depends on the finite performance of the period estimator $\hat{\theta}_{\hat{\lambda}}$. While the period estimator always hits the true period value, Table 3 aligns with the numerical results in Petersen and Müller (2019) and Zhou

and Müller (2022). Therefore, given a good estimation of θ_0 , the estimator $\hat{m}(t)$ can be expected to perform similarly to the standard estimator of the global Fréchet regression for $t = 1, \dots, T$. For this reason, we focus on the properties of $\hat{\theta}_{\lambda}$ in the remaining simulation studies for networks and functions in the Supplementary Material.

5. Real Data Analysis

5.1. U.S. Electricity Generation

We analyse the monthly composition of U.S. electricity generation using data from <https://www.eia.gov/electricity/data/browser/>. The data is preprocessed into a compositional form, where each entry in the compositional vector represents the percentage contribution of a specific energy source to net electricity generation. Following the same preprocessing idea in Dubey and Zheng (2023), we consolidate similar resource categories, resulting in seven broad groups: Coal; Petroleum (including petroleum liquids and petroleum coke); Gas (natural and other gases); Nuclear; Conventional hydroelectric; Renewables (wind, geothermal, biomass, and other renewables); and Solar (encompassing small-scale solar photovoltaic and all utility-scale solar). Our dataset consists of $T = 264$ monthly observations spanning from January 2001 to December 2022. Notably, each observation Y_t takes values a six-simplex $\Delta^6 = \{\boldsymbol{\delta} = (\delta_1, \dots, \delta_7)^\top \in \mathbb{R}^7 : \sum_{l=1}^7 \delta_l = 1 \text{ and } \delta_p > 0 \text{ for } p = 1, \dots, 7\}$. Similar to the simulation of compositional data in Section 4.2, we consider the square root transformation for compositional data, resulting in spherical data and choosing the corresponding metric be the geodesic distance

Applying our proposed methodology, we identify a periodicity of 12 months in U.S. monthly electricity generation compositions, as shown in Figure 6(a). Figure

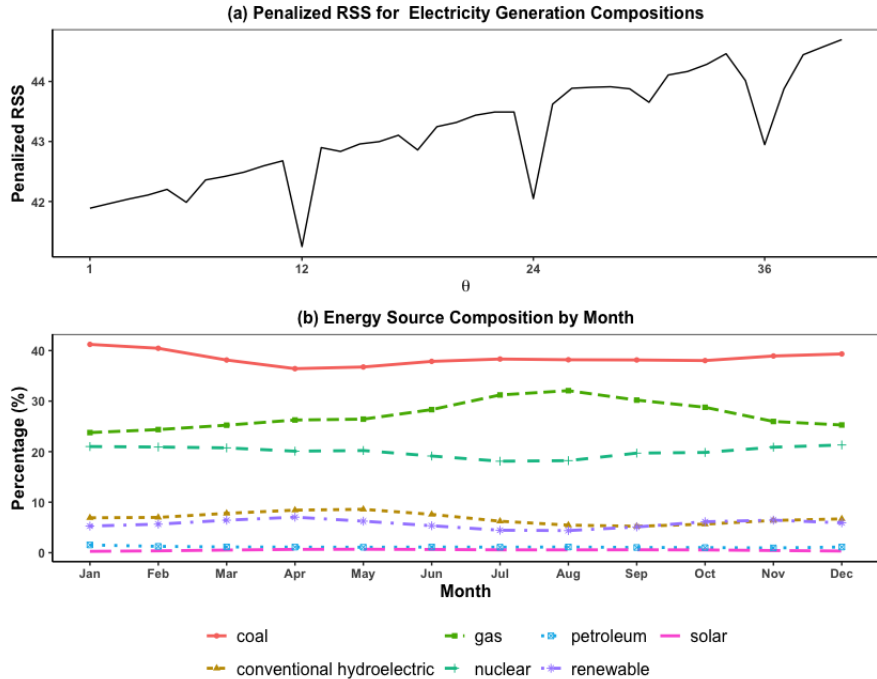


Fig. 6: (a) Plot of the penalized RSS with the selected tuning parameter for the monthly electricity generation compositions in U.S. (b) Plot of the elements of the estimated periodic component of the monthly electricity generation compositions in U.S..

6(a) shows that the penalized RSS exhibits distinct sharp drops around the period 12 and its multiples, indicating a yearly periodic pattern in electricity generation compositions.

We next turn to the estimation of the periodic component $m(t)$ for $t = 1, \dots, \theta_0$. Using the estimated period $\hat{\theta}_\lambda = 12$, we obtain the estimation via (9). Figure 6(b) illustrates the evolution of each energy source's percentage based on the estimation over time. The figure reveals clear seasonal trends in energy composition and provides meaningful insights. Notably, the percentage of gas peaks between July and September, aligning with increased summer demand and the fact that natural gas has become the dominant source of electricity generation in the U.S. Meanwhile,

coal consistently reaches its highest share at the beginning of each year. Conventional hydroelectric and renewable energy sources show higher percentages around April and lower around August. Moreover, the proportion of nuclear decreases in July and August, mainly due to the higher temperature in summer and nuclear power plants relying on water for cooling. In the summer, higher water temperatures can reduce cooling efficiency, forcing plants to lower output to maintain safe operating conditions.

5.2. New York City Citi Bike Sharing System

The New York City Citi Bike sharing system contains historical bike trip data, accessible at <https://citibikenyc.com/system-data>. This public dataset records trip start and end times, along with corresponding locations, at a second-resolution level, covering rides between bike stations throughout New York City.

Our study focuses on trips recorded over 15 weekdays in November 2019 to analyse the periodicity of time-varying transportation networks. By examining the hourly dynamics of bike rides across various stations, we aim to identify periodic patterns within the Citi Bike system and broader transportation trends. We consider the 90 most frequently used bike stations and segment each day into 24 one-hour intervals. For each one-hour interval, we construct a network with 90 nodes representing the selected stations, where edge weights indicate the number of trips between station pairs. This approach results in a time-varying network spanning 15 weekdays, from November 4 to November 22, 2019, yielding a total of 360 observations.

Each observation corresponds to a 90×90 graph Laplacian matrix that encapsulates the network among the 90 bike stations for a given one-hour period. For a network with 90 nodes, the graph Laplacian matrix L is obtained as $L = D - A$,

where A is the 90×90 adjacency matrix, with the (i, j) -th element a_{ij} being the edge strength between stations i and j , and D is a diagonal matrix with diagonal elements $d_{ii} = \sum_{j=1}^p a_{ij}$. The graph Laplacian provides a distinctive representation of the network structure. The metric we consider for the network Laplacians is the Frobenius metric.

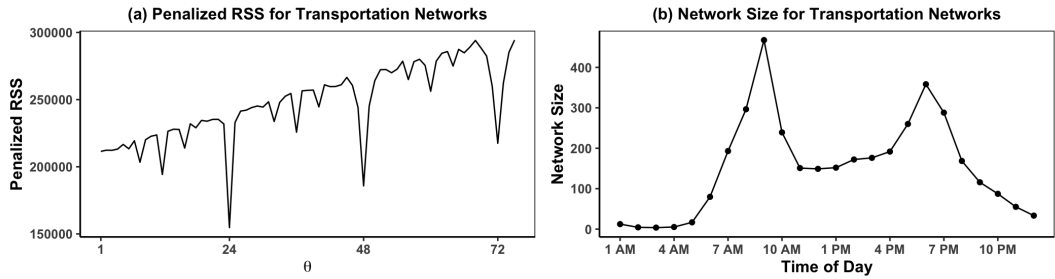


Fig. 7: (a) Plot of the penalized RSS with the selected tuning parameter for hourly transportation networks in New York City Citi Bike Sharing system. (b) Plot of the network sizes of the estimated periodic component of the hourly transportation networks in New York City Citi Bike Sharing system.

In what follows, we apply our proposed methodology to estimate the unknown period of the transportation networks. Once the period is estimated, we proceed to estimate the periodic component of the transportation networks. Figure 7(a) displays the penalized RSS with the selected tuning parameter for the hourly transportation data. The most notable feature is the noticeable dips with a global minimum at $\theta = 24$, along with additional spikes at its multiples. As discussed in Sections 2.2 and 4, such spikes are indicative of the presence of a periodic pattern in the data. The sharpness of the spike and the shape of the penalized RSS strongly suggest a periodic pattern with a period of 24 in the hourly transportation networks of the New York City Citi Bike Sharing system. Figure 7(a) indicates that there exists a

daily pattern for the hourly transportation networks, which has been observed in [Xu et al. \(2025\)](#).

To further analyse the periodic component, we consider to visualize the estimated periodic component by calculating the network size of the estimated periodic component at each time t , as illustrated in Figure 7(b). The figure reveals distinct peaks at 9 am and 6 pm, corresponding to morning and evening commuting surges, respectively. This result demonstrates that our proposed methodology effectively captures and quantifies periodicity in hourly transportation networks, as further supported by the interpretable patterns in Figure 7(b).

5.3. Water Consumption in Germany

We analyse daily functional water consumption in Germany using a dataset containing time-resolved measurements of water usage (in cubic meters) recorded hourly from January 2016 to March 2016. These measurements were collected at a pumping station within a regional water supply network, serving a mix of residential, commercial, and industrial consumers. To facilitate analysis, we preprocess the daily observations into a functional form, where each function represents the hourly water consumption pattern for a given day. After the preprocessing, the data consists of $T = 70$ daily water consumption curves. Additionally, we focus on the shape of daily water consumption curves and normalize every curves. The metric we use after the normalization is the Wasserstein metric, the one used in Section S3.2 in the Supplementary Material.

After employing the proposed methodology, a period of 7 has been identified based on the penalized RSS shown in Figure 8. In this figure, we observe sharp decreases around the period 7 and its multiple, indicating a weakly periodic pattern in water consumption curves.

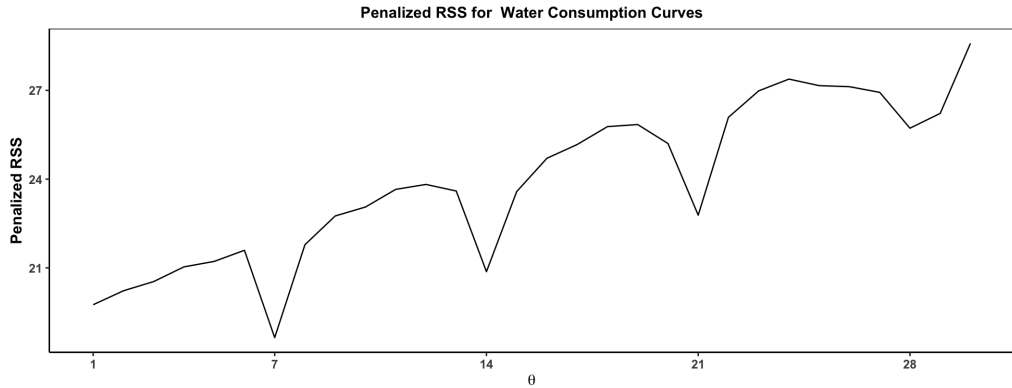


Fig. 8: Plot of the penalized RSS with the selected tuning parameter for the daily water consumption curves in Germany.

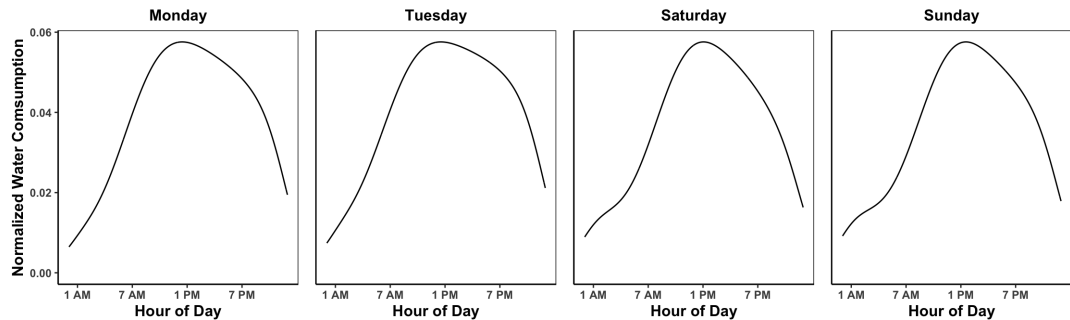


Fig. 9: Plots of the part of the estimated periodic component of the normalized daily water consumption curves in Germany. The estimated periodic component has a period 7 and contains 7 curves while 4 curves are given here.

Turning to the periodic component estimation, Figure 9 presents 4 of 7 curves in the estimated periodic component, the first two represent the weekday water consumption curves while the last two represent the weekend curves. The plots of all the elements in the estimated periodic component can be found in Figure S6 in the Supplementary Material. A clear periodic pattern can be observed in Figure 9. Notably, the daily water consumption curves have similar shapes on weekdays and weekends, respectively. For weekday consumption curves, peaks occur

before 1 pm while the peaks of weekend consumption curves happen after 1 pm. Notably, water consumption exhibits a smooth increasing trend starting early in the morning on weekdays while the increase appears less steep for weekends in the morning, especially on Sunday. The variations in morning and early afternoon water consumption are consistent with the differences in daily routines between workdays and weekends.

6. Conclusion

We introduce a novel nonparametric framework for quantifying periodicity in a time-varying random object within a general metric space that may lack local or global linear structures. Our approach formulates periodicity estimation as a model selection problem and provides methodologies for period estimation, data-driven tuning parameter selection, and periodic component extraction. Notably, our method offers a powerful tool for quantifying periodicity in random objects, an area that remains largely unexplored in a general object data setting.

Our theoretical contributions include establishing the consistency of period estimation without relying on linearity assumptions inherent in classical regression, providing rigorous support for data-driven tuning parameter selection, and deriving uniform convergence results for periodic component estimation.

Through extensive simulation studies and real data analysis spanning three distinct types of time-varying random object data, including networks, compositional data, and functional data, we demonstrate the superior accuracy of our approach in periodicity quantification and underscore its practical relevance in detecting and quantifying periodic patterns. With its versatility and minimal

parameter requirements, our approach holds significant potential for broad applications across diverse domains.

Appendix

Assumption A1 For each $t = 1, \dots, T$ and $\theta = 1, \dots, \Theta_T$, each barycenter $m_{F,t}(\theta, T)$ given in (4) exists, and

$$\inf_{\omega \in \Omega : d(\omega, m_{F,t}(\theta, T)) > \gamma} M_{F,t}(\omega; \theta, T) - M_{F,t}(m_{F,t}(\theta, T); \theta, T) > 0$$

for all $\gamma > 0$, where $M_{F,t}(\omega; \theta, T)$ is defined in (4).

Assumption A2 For $I(\zeta) = \int_0^1 \sqrt{\log N(\delta\zeta, B_\zeta(m_{F,t}(\theta, T)), d)} d\delta$, it holds that $I(\zeta) = O(1)$ as $\zeta \rightarrow 0$ for each $t = 1, \dots, T$ and $\theta = 1, \dots, \Theta_T$, where $B_\zeta(m_{F,t}(\theta, T)) = \{\omega \in \Omega : d(\omega, m_{F,t}(\theta, T)) < \zeta\}$ is the ζ -ball around $\mu_{GM}(t)$ and $N(\gamma, B_\zeta(m_{F,t}(\theta, T)), d)$ is the covering number.

Assumption A3 There exists $\rho > 0$, $D_1 > 0$ and $\beta_1 > 1$ such that whenever $\omega \in \Omega : d(\omega, m_{F,t}(\theta, T)) < \rho$,

$$M_{F,t}(\omega; \theta, T) - M_{F,t}(m_{F,t}(\theta, T); \theta, T) - D_1 d^{\beta_1}(\omega; m_{F,t}(\theta, T)) \geq 0,$$

holds for each $t = 1, \dots, T$ and $\theta = 1, \dots, \Theta_T$.

Assumption A4 For all $\gamma > 0$,

$$\inf_{\substack{1 \leq \theta \leq \Theta_T \\ 1 \leq t \leq T}} \inf_{\omega \in \Omega : d(\omega, m_{F,t}(\theta, T)) > \gamma} M_{F,t}(\omega; \theta, T) - M_{F,t}(m_{F,t}(\theta, T); \theta, T) > 0.$$

Moreover, there exists $\aleph = \aleph(\gamma) > 0$ such that

$$\mathbb{P} \left(\inf_{\substack{1 \leq \theta \leq \Theta_T \\ 1 \leq t \leq T}} \inf_{\omega \in \Omega: d(\omega, \hat{m}_{F,t}(\theta, T)) > \gamma} \hat{M}_{F,t}(\omega; \theta, T) - \hat{M}_{F,t}(\hat{m}_{F,t}(\theta, T); \theta, T) \geq \aleph \right) \rightarrow 1$$

Assumption A5 For the ζ -ball around $\mu_{\text{GM}}(t)$, $B_\zeta(m_{F,t}(\theta, T)) = \{\omega \in \Omega : d(\omega, m_{F,t}(\theta, T)) < \zeta\}$, and the covering number, $N(\gamma, B_\zeta(m_{F,t}(\theta, T)), d)$, satisfies

$$\int_0^1 \sup_{\substack{1 \leq \theta \leq \Theta_T \\ 1 \leq t \leq T}} \sqrt{\log N(\delta\zeta, B_\zeta(m_{F,t}(\theta, T)), d)} d\delta = O(1),$$

as $\zeta \rightarrow 0$.

Assumption A6 There exists $r > 0$, $D_2 > 0$ and $\beta_2 > 1$ such that

$$\inf_{\substack{1 \leq \theta \leq \Theta_T \\ 1 \leq t \leq T}} \inf_{\omega \in \Omega: d(\omega, m_{F,t}(\theta, T)) < r} \left\{ M_{F,t}(\omega; \theta, T) - M_{F,t}(m_{F,t}(\theta, T); \theta, T) - D_2 d^{\beta_2}(\omega; m_{F,t}(\theta, T)) \right\} \geq 0.$$

Assumption A1 includes an identifiability condition for the population conditional barycenter, which is an M -estimator. Moreover, Assumption A1 guarantees the existence of these barycenters for all $t = 1, \dots, T$. Related discussions can be found in [Sturm \(2003\)](#) and [Ahidar-Coutrix et al. \(2020\)](#). The identifiability condition Assumption A1 can be used to ensure the uniqueness of these barycenters. Notably, we do not require the uniqueness of the sample version of these barycenters, compared to the assumptions used in [Petersen and Müller \(2019\)](#) and [Zhou and Müller \(2022\)](#). To see this, note that any choice of the point $\hat{m}_{F,t}(\theta, T)$ in the set of the sample barycenters is the exact minimizer of the cost function $\hat{M}_{F,t}(\omega; \theta, T) =$

$T^{-1} \sum_{i=1}^T s_i^{(t)} d^2(Y_i, \omega)$. Therefore, one can see that the required condition to derive the convergence of an M -estimator (van der Vaart and Wellner 1996) such as $\hat{M}_F(\hat{m}_{F,t}(\theta, T); \theta, T) \leq \inf_{\omega \in \Omega} \hat{M}_F(\omega; \theta, T) + o_p(1)$ is satisfied. Assumption A2 is a bound on the covering number, defined e.g. in van der Vaart and Wellner (1996), of the object metric space and is satisfied by a variety of random objects. Assumption A3 is a standard requirement for M -estimators, which characterizes the local curvature of the cost function near its minimum. The curvature is characterized by β_1 , which controls the convergence rate of the empirical conditional barycenter $\hat{m}_{F,t}(\theta, T)$ for each $t = 1, \dots, T$. Assumptions A1-A3 are consistent with those used in deriving the pointwise convergence of the conditional barycenters (see Petersen and Müller (2019) and Zhou and Müller (2022)) by noting that these population and empirical barycenters are the population and empirical Fréchet regression estimators, respectively. Assumptions A4-A6 are the uniform versions of Assumptions A1-A3, respectively. Assumptions A4-A6 are consistent with those used in deriving the uniform convergence of the conditional barycenters (see Petersen and Müller (2019) and Zhou and Müller (2022)). To see this, in the proof of Lemma S2 in the Supplementary Material, we can represent the population and empirical barycenters using the same notations to those used for the Fréchet regression estimators in Petersen and Müller (2019). Object spaces that meet these conditions include graph Laplacian matrices with the Frobenius metric, univariate probability distributions with the 2-Wasserstein metric, and spherical data with geodesic distance (see Petersen and Müller (2019)).

Acknowledgements

ATAW acknowledges with thanks support from Australian Research Council grant DP220102232.

References

Ahidar-Coutrix, A., Le Gouic, T., and Paris, Q. (2020). Convergence Rates for Empirical Barycenters in Metric Spaces: Curvature, Convexity and Extendable geodesics. *Probability Theory and Related Fields* 177, 323–68.

Bai, J. and Ng, S. (2002). Determining the Number of Factors in Approximate Factor Models. *Econometrica*, 70(1), 191–221.

Chen, J. and Chen, Z. (2008). Extended Bayesian Information Criteria for Model Selection with Large Model Spaces. *Biometrika*, 95(3), 759–771.

Claeskens, G. and Hjort, N. L. (2008). *Model Selection and Model Averaging*. Cambridge books. Cambridge University Press.

Dubey, P. and Müller, H.-G. (2021). Modeling Time-Varying Random Objects and Dynamic Networks. *Journal of the American Statistical Association*, 117, 2252–67.

Dubey, P. and Zheng, M. (2023). Change Point Detection for Random Objects Using Distance Profiles. *arXiv preprint arXiv:2311.16025*.

Fréchet, M. (1948). Les éléments aléatoires de nature quelconque dans un espace distancié. *Annales de l'institut Henri Poincaré*, 10(4), 215–310.

Guo, L. and Modarres, R. (2020). Nonparametric Change Point Detection for Periodic Time Series. *Canadian Journal of Statistics*, 48(3):518–534.

Hall, P., Reimann, J., and Rice, J. (2000). Nonparametric Estimation of a Periodic Function. *Biometrika*, 87(3):545–557.

Hörmann, S., Kokoszka, P., and Nisol, G. (2018). Testing for Periodicity in Functional Time Series. *The Annals of Statistics*, 46(6A):2960–2984.

Kolar, M., Song, L., Ahmed, A., and Xing, E. P. (2010). Estimating Time-Varying Networks. *The Annals of Applied Statistics*, 94–123.

Mallows, C. L. (1973). Some Comments on C_p . *Technometrics*, 15, 661–675.

Mardia, K.V., Kent, J.T. and Bibby, J.M. (1979) *Multivariate Analysis*. Academic Press.

Marron, J. S. and Dryden, I. L. (2021). *Object Oriented Data Analysis*. Chapman and Hall/CRC.

Petersen, A. and Müller, H.-G. (2019). Fréchet Regression for Random Objects with Euclidean Predictors. *The Annals of Statistics*, 47(2):691–719.

Quinn, B. G. and Thomson, P. J. (1991). Estimating the Frequency of a Periodic Function. *Biometrika*, 78(1):65–74.

Rice, J. A. and Rosenblatt, M. (1988). On Frequency Estimation. *Biometrika*, 75(3):477–484.

Scealy, J. and Welsh, A. (2011). Regression for Compositional Data by Using Distributions Defined on the Hypersphere. *Journal of the Royal Statistical Society: Series B (Statistical Methodology)*, 73(3):351–375.

Scealy, J. L. and Wood, A. T. A. (2023). Score Matching for Compositional Distributions. *Journal of the American Statistical Association*, 118(543):1811–1823.

Schwarz, G. (1978). Estimating the Dimension of a Model. *The Annals of Statistics*, 6(2): 461–464.

Sturm, K.-T. (2003). Probability Measures on Metric Spaces of Nonpositive Curvature. *Heat Kernels and Analysis on Manifolds, Graphs, and Metric Spaces: Lecture Notes from a Quarter Program on Heat Kernels, Random Walks, and Analysis on Manifolds and Graphs: April 16-July 13, 2002, Emile Borel Centre of the Henri Poincaré Institute, Paris, France*, 338–357.

Sun, Y., Hart, J. D., and Genton, M. G. (2012). Nonparametric Inference for Periodic Sequences. *Technometrics*, 54(1):83–96.

Tucker, D. C., Wu, Y., and Müller, H.-G. (2023). Variable Selection for Global Fréchet Regression. *Journal of the American Statistical Association*, 118(542):1023–1037.

van der Vaart, A. and Wellner, J. (1996). *Weak Convergence of Empirical Processes: With Applications to Statistics*. New York: Springer.

Vogt, M. and Linton, O. (2014). Nonparametric Estimation of a Periodic Sequence in the Presence of a Smooth Trend. *Biometrika*, 101(1):121–140.

Walker, A. M. (1971). On the Estimation of a Harmonic Component in a Time Series with Stationary Independent Residuals. *Biometrika*, 58(1):21–36.

Wang, H., Li, B., and Leng, C. (2009). Shrinkage Tuning Parameter Selection With a Diverging Number of Parameters. *Journal of the Royal Statistical Society Series B: Statistical Methodology*, 71(3), 671–683.

Wang, J.-L., Chiou, J.-M., and Müller, H.-G. (2016). Functional Data Analysis. *Annual Review of Statistics and Its Application*, 3(1), 257–295.

Wang, S., Huang, T., You, J., and Cheng, M.-Y. (2022). Robust Inference for Nonstationary Time Series with Possibly Multiple Changing Periodic Structures. *Journal of Business & Economic Statistics*, 40(4):1718–1731.

Worsley, K. J., Liao, C. H., Aston, J., Petre, V., Duncan, G., Morales, F., and Evans, A. C. (2002). A General Statistical Analysis for fMRI Data. *Neuroimage*, 15(1):1–15.

Xu, J., Wood, A. T. A., and Zou, T. (2025). Change Point Detection for Random Objects with Possibly Periodic Behavior. *arXiv preprint arXiv:2501.01657*.

Zhang, T. (2025). Penalty Free Variable Selection for High-Dimensional Linear Models. *Electronic Journal of Statistics*, 19(1), 2803–2828.

Zhou, Y. and Müller, H.-G. (2022). Network Regression with Graph Laplacians. *Journal of Machine Learning Research*, 23(320), 1–41.